Overpressure generation by smectite dehydration in sedimentary basins constrained by salinity dilution and stable isotopes

Joachim Tremosa, Eric Gaucher, Hélène Gailhanou

Version of Record: https://www.sciencedirect.com/science/article/pii/S0883292721001670
Manuscript_3912c2b2d13cd59a3113d4c4cce0ef8e

Overpressure generation by smectite dehydration in sedimentary basins constrained by salinity dilution and stable isotopes

Joachim Tremosa[1], Eric C. Gaucher[2], Hélène Gailhanou[1]*

1. BRGM, 3 avenue Claude Guillemin, BP 36009, 45060 Orléans, France

2. TOTAL S.A., CSTJF, Avenue Larribau, 64018 Pau, France

**corresponding author: j.tremosa@brgm.fr; (phone n°: +33238643204)*

Graphical abstract

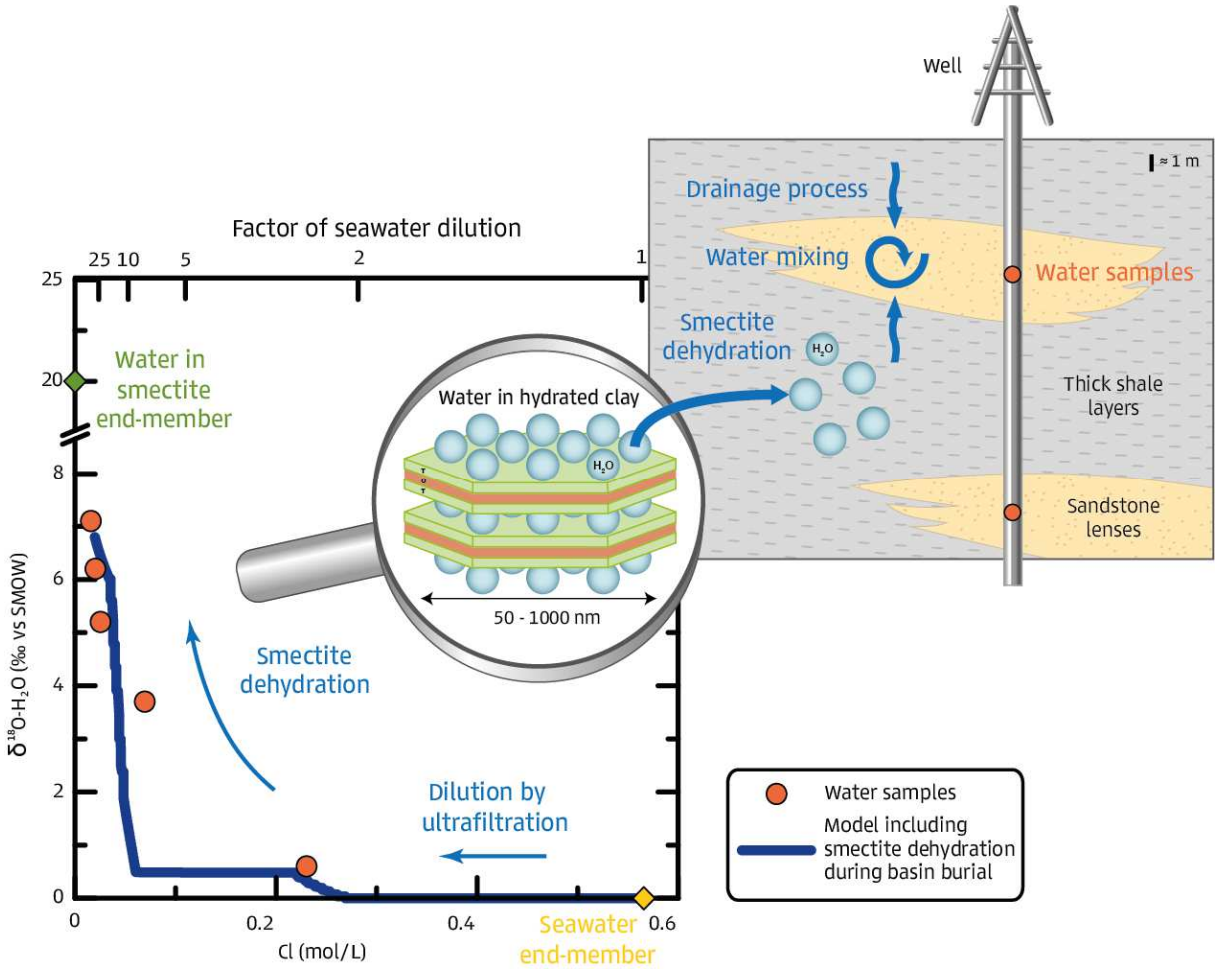

Abstract

The water released by smectite dehydration because of pressure and temperature increase during burial of claystone or clay-rich mudstone in sedimentary basins can generate overpressure and change the water salinity. Up until now, a clear distinction has been lacking between the water fraction produced by compaction and the water fraction produced by thermodynamic dehydration. Smectite dehydration is mentioned in the literature in pore pressure prediction or as a hypothesis for water freshening but direct evidence is missing.

Here, we bring this evidence by linking the $\delta^{18}O$-H_2O water isotopic signature, salinity evolution and overpressure generation to the spatial and temporal fluid budget in a sedimentary pile involving smectite dehydration. Water samples indicating an increase in $\delta^{18}O$-H_2O and a salinity decrease were sampled deep offshore in the Gulf of Guinea in sandstone lenses intercalated within shale layers. By using a numerical coupled approach, we were able to reproduce the fluid evolution by modelling smectite dehydration based on thermodynamic considerations during the burial of the sedimentary pile and the associated pressure and temperature evolution over geological ages.

Introduction

An understanding of fluid migration and trapping over the history of sedimentary basins is needed for the sustainable and cost-effective exploitation of geothermal and oil and gas subsurface resources as it ensures a more accurate evaluation of the resource and anticipation of its evolution. In deep geological settings considering the impact of clay-rich sediments on the fluid migration and pressure evolution remain a challenge. Migration of fluids and solutes is complexly impacted in deep claystones because of their low permeability, their membrane behaviour that can restrict the transport of waters and solutes and because of the water/rock interactions.

Smectite dehydration in sedimentary basins is sometimes cited as a process that can generate abnormal pressure conditions (Audet, 1995; Bruce, 1984; Tanikawa et al., 2008; Tremosa et al., 2020) or as a freshening mechanism. However, direct evidence of the influence of smectite dehydration on fluid evolution at the scale of the basin or formation was still missing. Smectite dehydration consists in the loss of interlayer water within smectite crystal that occurs with temperature and pressure increase (Figure 1). The term ‘smectite dehydration’ also refers to the loss of water during the smectite-to-illite transformation and attention was mainly paid to this latter process in sedimentary basins. In both cases, when smectite dehydration of interlayer water occurs or when the smectite structure evolves to an illite structure, the interlayer water is released to the shale porosity. The

smectite dehydration process must not be confused with the water produced by the compaction of the clayey formations. In the latter process, interstitial water is drained by applying burial stress to the formations.

Overpressures in sedimentary basins are hydrodynamic phenomena involving various coupled geological processes over the basin history (Neuzil, 1995). When the different hydraulic, mechanical, thermal and chemical couplings are considered, the interpretation of overpressure generation and dissipation to obtain the present-day pressure profile provides good insights into the fluid migration and budget in the basin. At the basin scale, the expression of smectite dehydration can be recorded by the pore pressure (Bruce, 1984; Tanikawa et al., 2008; Tremosa et al., 2020), but the interpretation of the origin of the pore pressure profile generally remains uncertain (Bjørlykke et al., 2010) with smectite dehydration acting as an additional cause of overpressure (Audet, 1995; Tremosa et al., 2020). Stable oxygen isotopic data are also commonly used to document the pore fluid history in sedimentary basins (Hanor, 1994), taking into account the contribution of the different sources of water. Pore fluid enriched in ^{18}O concomitantly to a decrease in salinity is often interpreted as the consequence of smectite dehydration (Boschetti et al., 2016; Clayton et al., 1966; Franks & Uchytil, 2016; Macpherson, 1992; Morton & Land, 1987; Nicot et al., 2018; Wilkinson et al., 1992). However, this interpretation of smectite dehydration influencing the $\delta^{18}O\text{-}H_2O$ isotopic signature and salinity is generally not based on a volume budget of water released by smectite minerals and its mixing with porewater in the sedimentary pile. Moreover, the thermodynamics of smectite dehydration are rarely checked (Colten-Bradley, 1987; Vidal & Dubacq, 2009). Consequently, the effect of smectite dehydration remains a hypothesis that requires to be tested by a coupled approach, combining burial, smectite dehydration and water freshening considerations.

Smectite dehydration is also documented in mud volcanoes (Dählmann & Lange, 2003; Hensen et al., 2007) and in subduction zones (Kastner et al., 1993), where correlations are observed between water freshening and an increase in the $\delta^{18}O\text{-}H_2O$ isotopic signature, and are explained by smectite dehydration. These studies generally relate water release to smectite-to-illite transformation, but a few of them focus on the dehydration of interlayer smectite (Fitts & Brown, 1999; Hüpers & Kopf, 2012). In these studies, smectite dehydration was induced in laboratory experiments that considered pressure and temperature conditions of convergent margins. In subduction zones and mud volcanoes, smectite dehydration during illitisation has also been considered in the fluid budget of numerical analyses to explain the observed water freshening with depth (Bekins et al., 1995; Brown et al., 2001; Henry & Bourlange, 2004; Hüpers et al., 2019; Saffer & McKiernan, 2009; Vanneste et al., 2011). However, these studies only consider the temperature dependence of the smectite-to-illite transformation, overlooking smectite dehydration.

In our study, we tested the effect of smectite dehydration on the $\delta^{18}O$-H_2O isotopic signature, the evolution of pore fluid salinity and overpressure generation in a sedimentary pile in the Gulf of Guinea. The $\delta^{18}O$-H_2O signature and the salinity are two records of smectite dehydration and of the volume of water that is consequently released in the sediments. Smectite dehydration is described by considering a consistent thermodynamic model as a function of pressure and temperature evolution during the burial of the sedimentary pile. The water budget then accounts for the release of water by smectite dehydration depending on the geometry, pressure, temperature and properties of the sedimentary pile and the timing of this water release.

Methods

Sampling and analyses

Field data were obtained from a well, drilled to explore the petroleum potential of the Gulf of Guinea. This well is located about 50 km from the coast, at a sea depth of about 2000 m. The drilling penetrated through a sediment thickness of about 2700 m, from the seafloor. The main objective of the well was to identify the Upper Cretaceous post-rift series and, in particular, the sandstone reservoirs in turbidite systems. During the drilling operations and the following tests, a large set of data was obtained regarding geology, lithology, mineralogy, pressure and temperature conditions and fluid composition in the reservoirs, amongst other information. The following data from the well were used for hydrogeological interpretation and the modelling of the present study:

- The lithological and composite logs of the well at a scale of 1:500 were used to establish the lithological profile and the meshing.
- Biostratigraphic dating was available, based on foraminifera, nanoplankton and pollens identified on cuttings and cores. This dating was used together with the sediment thickness at the deposition to calculate the sedimentation rate.
- The formation pressure, corresponding to the fluid pressure, was measured in the well by 87 measurements using Schlumberger Modular Formation Dynamics Tester of which 28 gave good quality results. The pressure was hydrostatic down to the Campanian deposit basis. A moderate fluid overpressure was measured below, corresponding to an apparent density of 1250 to 1300 kg.m^{-3} in Turonian and Santonian levels ($\rho = {}^{P}/_{g \,.\, z}$). The Turonian reservoirs separated by shale layers are not hydraulically connected. In addition, the shale pressure was measured to be close to the reservoir pressure.
- A temperature gradient of about 4.4 °C/100 m was measured between the seabed (4 °C) and the well foot during electrical logs.

- The mineralogy and petrography of samples presenting different facies and ages were determined through petrographic studies on 43 samples, by quantitative mineralogy analyses (bulk rock XRD-XRF, CEC, density, organic carbon and sulphur analyses and XRD clay fraction analyses) on 66 samples and by complementary mineralogical analyses on clay mineral phases (electron microprobe) on 3 samples.
- Five water samples were taken during MDT tests in the sandstone reservoir at depths between 2000 and 2600 m below the seafloor, allowing the determination of the chemical and isotopic ($\delta^{18}O$ and $\delta^{2}H$-H_2O, $^{87}Sr/^{86}Sr$, $\delta^{34}S$ and $\delta^{18}O$-SO_4 and $\delta^{7}Li$) composition of these waters.

Thermodynamic model for smectite dehydration

The chemical composition of pure smectite was determined for a shale sample of the Turonian age from the well, by performing 150 electron microprobe analyses on the < 2 µm clay fraction. Among them, the smectite compositions, expressed on a structural basis of $O_{10}(OH)_2$, were selected using M^+-4Si-R^{2+} diagrams (Meunier & Velde, 1989) (M^+ = layer charge of ideal micas, 4Si = maximum Si content of the tetrahedral sheet, R^{2+} = amount of bivalent cations in the octahedral position), following which the compositions associated with mixtures of clay minerals and/or other silicate minerals could be discarded. The following mean composition for smectite was obtained $(Na_{0.085}K_{0.180}Ca_{0.037})(Si_{3.809}Al_{0.191})(Al_{1.720}Mg_{0.090}Fe^{2+}_{0.256})O_{10}(OH)_2$, with a molar mass of 379.51 g/mol. For sake of simplicity in the application of the thermodynamic model in the burial model, the Na homoionized form of the smectite was considered.

The thermodynamic smectite dehydration model (Vidal & Dubacq, 2009) adapted for use in PHREEQC geochemical calculation code (Tremosa et al., 2020) considers binary solid solutions between hydrated smectite end-members with 1, 2 or 3 layers of water, which respectively contain 2, 4 and 7 moles of interlayer water per mole of smectite (on a structural basis $O_{10}(OH)_2$), and anhydrous smectite. The description of smectite dehydration then involves the three following binary solid solutions, where A refers to anhydrous, and 1w, 2w and 3w refer to 1, 2 and 3 layers of water, respectively:

- Smect_Na.A – Smect_Na.1w
- Smect_Na.A –Smect_Na.2w
- Smect_Na.A –Smect_Na.3w

The deployment of this smectite dehydration model required calculating the thermodynamic properties (*G*, *H*, *S*, C_p, *V*) of the anhydrous end-member (Blanc et al., 2015) and of the hydrated smectite end-members (Vidal & Dubacq, 2009) (Table 1) as well as the dependence of the smectite equilibrium constant on temperature (Table 2). The interaction parameters of the non-ideal solid solution estimated for montmorillonites were used (Vidal & Dubacq, 2009). So, Margules parameters of -10 kJ are considered for solid solutions between anhydrous smectite and the three hydrated smectite end-members.

Preferential stability domains of the different hydrated smectite end-members were calculated depending on the pressure and temperature conditions. The transition pressure and temperature from a hydrated smectite end-member to a less hydrated smectite were then determined and used in the model coupling burial and dehydration. For a given smectite, three stability domains were then defined corresponding to the pressure and temperature conditions where the solid solution with 3 layers of water, 2 layers of water and 1 layer of water are in play. The stability domains for Na smectite from the sedimentary pile are delimitated by the following functions:

- Transition Smect_Na.3w → Smect_Na.2w according (P_{tr1},T_{tr1}) :

  $P_{tr1} = 102.53\ T_{tr1} - 2843.9$ ($r^2 = 0.990$)

- Transition Smect_Na.2w → Smect_Na.1w according (P_{tr2},T_{tr2}) :

  $P_{tr2} = 201.25\ T_{tr2} - 20942$ ($r^2 = 0.968$)

, with P_{tr} expressed in bar and T_{tr} in °C.

Table 1 : Thermodynamic properties estimated for the smectite identified in the well and expressed as Na homoionized smectite at 1.013 bar and 298.15 K. Clay mineral Cp(T) functions are expressed as $C_p(T) = A + B.10^{-3}\ T + C\ 10^5\ T^{-2}$, where A, B and C are Maier-Kelley coefficients.

	$m_n H_2O$	$\Delta G_f°$	$\Delta H_f°$	$\delta H_f° m_n H_2O$	$S°$	$V°$	C_p(25°C)	*A*	*B*	*C*
	(mol/O_{10})	kJ/mol	kJ/mol	kJ/mol	J/mol/K	cm^3/mol	J/mol/K	J/mol/K	J/mol/K^2	J/mol*°K
Smect_Na.A	0	-5277.00	-5641.05		293.60	134.32	314.25	329.41	235.20	-75.82
Smect_Na.1w	2	-5762.50	-6232.85	293.85	403.60	168.56	402.23	418.09	284.52	-89.50
Smect_Na.2w	4	-6239.71	-6816.35	291.75	513.60	202.81	490.21	506.76	333.84	-103.19
Smect_Na.3w	7	-6951.26	-7687.34	290.33	678.60	250.75	622.19	639.77	407.82	-123.72

Table 2 : Temperature dependence of the equilibrium constant (log_{10} K) for the dissolution of the identified Na smectite in water, at 298.15 K and 1.013 bar. $log_{10}K = A_1 + A_2*T + A_3/T + A_4*log(T) + A_5/T^2$

	$m_n H_2O$	$log_{10}K$	A1	A2	A3	A4	A5	Dissolution reaction
Smect_Na.A	0	4.78	-1.2871864E+03	-2.2190924E-01	6.9174286E+04	4.6807708E+02	-2.8539614E+06	$Na_{0.339}(Si_{3.809}Al_{0.191})(Al_{1.72}Mg_{0.09}Fe_{0.256})O_{10}(OH)_2$ + $6.764H^+$ + $3.236H_2O$ = $1.911Al^{+++}$ + $0.256Fe^{++}$ + $0.09Mg^{++}$ + $0.339Na^+$ + $3.809H_4SiO_4$

Smect_Na.1w	2	2.82	-1.2400371E+03	-2.1299471E-01	6.5227041E+04	4.5146250E+02	-2.6249665E+06	$Na_{0.339}(Si_{3.809}Al_{0.191})(Al_{1.72}Mg_{0.09}Fe_{0.256})O_{10}(OH)_2$:$2H_2O$ + $6.764H^+$ + $1.236H_2O$ = $1.911Al^{+++}$ + $0.256Fe^{++}$ + $0.09Mg^{++}$ + $0.339Na^+$ + $3.809H_4SiO_4$
Smect_Na.2w	4	2.30	-1.1928878E+03	-2.0408019E-01	6.1713440E+04	4.3484792E+02	-2.3959717E+06	$Na_{0.339}(Si_{3.809}Al_{0.191})(Al_{1.72}Mg_{0.09}Fe_{0.256})O_{10}(OH)_2$:$4H_2O$ + $6.764H^+$ = $1.911Al^{+++}$ + $0.256Fe^{++}$ + $0.09Mg^{++}$ + $0.339Na^+$ + $3.809H_4SiO_4$ + $0.764H_2O$
Smect_Na.3w	7	2.28	-1.1246081E+03	-1.9110531E-01	5.6792159E+04	4.1082120E+02	-2.0593250E+06	$Na_{0.339}(Si_{3.809}Al_{0.191})(Al_{1.72}Mg_{0.09}Fe_{0.256})O_{10}(OH)_2$:$7H_2O$ + $6.764H^+$ = $1.911Al^{+++}$ + $0.256Fe^{++}$ + $0.09Mg^{++}$ + $0.339Na^+$ + $3.809H_4SiO_4$ + $3.764H_2O$

Model coupling burial, dehydration and water freshening

The SURP code (Tremosa et al., 2020), a thermo-hydro-mechanical model coupled with chemical reactivity, was used to calculate the pore pressure evolution during the burial of a sedimentary pile under the combined effects of mechanical compaction, thermal expansion, water production by mineralogical reactions and water flow. This model relies on the resolution of the continuity equation in a porous medium where the variation of fluid mass depends on the changes in fluid pressure, mechanical stress and temperature over time. A source term is added to the water balance to consider the coupling with production and consumption of water by mineralogical reactions. The coupled flow equation can be expressed as follows:

$$Ss' \frac{\partial P}{\partial t} - Ss' \xi \frac{d\sigma_{zz}}{dt} - \rho_f g \Lambda' \frac{\partial T}{\partial t} = \nabla \left[g \frac{k \rho_f}{\mu_f} \left(\nabla P - \rho_f g \nabla z \right) \right] + \Gamma$$

where, S_s' is the unidimensional specific storage coefficient (m^{-1}), P is the pore pressure (Pa), t is the time (s), ξ is the unidimensional loading coefficient (dimensionless), σ_{zz} is the total vertical stress (Pa), ρ_f is the fluid density ($kg.m^{-3}$), g is the acceleration constant due to gravity (9.81 $m.s^{-2}$), Λ' is the thermal response coefficient ($°C^{-1}$), T is the temperature (°C), ∇z is (0,0,1) if the z axis is orientated downward, μ_f is the fluid dynamic viscosity (Pa.s) and Γ is a source term corresponding to input or withdrawal of water in the porosity.

The chemical and isotopic evolutions of the water in the sandstone reservoirs were calculated by reproducing the mixing of sandstone water with water coming from the surrounding shale layers. For that, the water produced by smectite dehydration in the cells of the underlying and overlying shale layers was summed and mixed as fresh water in the water filling the sandstone layer. This mixing was performed during the PHREEQC operations of the SURP Python-PHREEQC coupling, using the keyword 'MIX' and considering the following mixing factor $F_{mix}^{dehydration}$:

$$F_{mix}^{dehydration} = \frac{\sum mass\ of\ dehydration\ water}{sandstone\ thickness\ \times\ \rho_f\ \times n}$$

where, *n* is the porosity.

This mixing factor allows the evolution of the isotopic signature to be calculated by mixing the sandstone reservoir water which initially has a $\delta^{18}O\text{-}H_2O$ signature of 0 ‰, corresponding to connate seawater, with water released by smectite dehydration with a $\delta^{18}O\text{-}H_2O$ signature of +20 ‰ (Savin & Lee, 1988; Sheppard & Gilg, 1996). No isotopic fractionation was considered during dehydration reactions.

The dilution of sandstone reservoir water due to a flow of fresh water, i.e. by ultrafiltration in the shale or leakage, modifies the water salinity when the system becomes hydraulically closed. In this way, a dilution factor was applied to the water filling the sandstone reservoirs when the intrinsic permeability of the overlying shale layer was lower than 10^{-20} m². As long as the system was hydraulically open, it was assumed that the inflow of fresh water was equilibrated by advective mixing and a decrease in salinity cannot be observed. The dilution factor applied in the sandstone layer was adjusted to fit the observed salinity decrease.

The model mesh was built from the well log, and mineralogy and parameter profiles. The 2700 m thick sedimentary pile was divided into 82 successive lithological layers. The thickness of these lithological layers can vary between 2 m, for sandstone layers intercalated between shales, and 683 m, for shallow sediments not concerned by the mechanisms under study. A backstripping or decompaction model (Sclater & Christie, 1980) was applied to calculate the thickness of each lithological layer at the time of its deposit. The calculated thickness of the uncompacted sedimentary pile is about 4400 m. Each lithological layer was then sliced into several meshes if the thickness of the uncompacted layer was greater than 10 m. The geometry of the sedimentary pile is therefore described by 411 meshes of initial thickness varying between 2.2 and 19.4 m. Sedimentation rates (Table 3) were calculated from the uncompacted thickness of sediments and the biostratigraphic dating for the well. The most significant sedimentation event occurred during the Santonian age, with a sedimentation rate of 340 m/My.

Table 3: Sedimentation rates for forward modelling of IVOIRE-1X sediment deposition.

Geological age		**Sedimentation rate (m/My)**
Since Miocene	15.97 My to present	60
Middle Eocene and Oligocene	41.2 My to 15.97 My	0
Paleocene and Middle Eocene	66 My to 41.2 My	20.4
Campanian and Maastrichtian	83.6 My to 66 My	52.5
Santonian	86.3 My to 83.6 My	340.1
Coniacian	89.8 My to 86.3 My	34.8
Turonian	93.9 My to 89.8 My	47.7
Cenomanian	100.5 to 93.9 My	39.4
Albian	113 to 100.5 My	40

Hydraulic and mechanical calculation parameters and initial content in smectite are reported in Table 4. In terms of hydraulic boundary conditions, hydrostatic conditions are considered in the layers of the sedimentary pile above the roof of the measured overpressure. A no-flow Neumann boundary condition is taken on the basis of the modelled sedimentary pile. This model considers a constant temperature gradient with depth (0.0446 °C/m) based on the present-day geothermal gradient, which is a simplification.

Table 4: Calculation parameters used in SURP modelling. 'sh', 'shsd' and 'sd' respectively correspond to the 'shale', 'shaly-sandstone' and 'sandstone' facies encountered in the IVOIRE-1X sedimentary pile. n *is porosity and* e *is the void ratio.*

Intrinsic permeability *k* (m^2)	'sh' : $\boldsymbol{k = \frac{\left(\frac{n}{(1-n)\ 40 \times 2720}\right)^2}{3\ n^{-3}}}$ 'shsd' : $\boldsymbol{k = \frac{\left(\frac{n}{(1-n)\ 40 \times 2680}\right)^2}{3\ n^{-3}}}$ 'sd' : $\boldsymbol{k = 9.87\ 10^{-13} \times 0.03 n^3}$
Biot coefficient α (dimensionless)	$\alpha = 1 - (1-n)^{3.8}$
Poisson ratio ν (dimensionless)	$\nu = 0.3$
Young modulus *E* (GPa)	$E = 25(1-n)^{10}$
Compaction index C_c (dimensionless)	'sh' : $C_c = 0.7e + 0.44$ 'shsd' : $C_c = 0.5e + 0.4$ 'sd' : $C_c = 0.15e + 0.35$
Mineralogy	'sh': Smectite_Na 30 % 'shsd': Smectite_Na 15 % 'sd': Smectite_Na 0 %

Geological context – Sand lenses draining water produced in shale layers

Intercalations of sandstone lenses in thick shale layers of the Cenomanian, Turonian and Santonian ages were found in the transform margin context of the Gulf of Guinea (Antobreh et al., 2009; Mascle & Blarez, 1987). The exploration well is located offshore at a water depth of about 2000 m. The well is drilled through a sediment thickness of about 2700 m. Several sandstone lenses 3 to 20 m thick were intercalated between thicker shale layers 5 to 143 m thick in marine deposits corresponding to transgressive sequences during the first connections with the Tethysian domain, during the opening of the equatorial Atlantic Ocean. The sandstone corresponds to subarkose sandstones in the Folk

classification and present a porosity between 10 and 20 % for a permeability generally higher than 1 milliDarcy (10^{-15} m²). Shale layers consist in claystones composed of 30 to 45 % of clay minerals and mica, depending on the samples. Quartz and feldspars are the other main constituents. The smectite is montmorillonite showing octahedral substitutions. Permeability between 0.0005 and 0.1 milliDarcy were measured on the argillaceous sandstone facies but no measurements were made on samples richer in clay minerals of the claystone facies.

Figure 1 schematically presents the geometry of the sandstone lenses intercalated in thicker shale layers. The water released by the shales drains into the sandstone lenses where mixing with the initial porewater can occur. It is therefore thought that information on the fluid evolution can be deduced from water samples taken in the sandstone lenses at different depths.

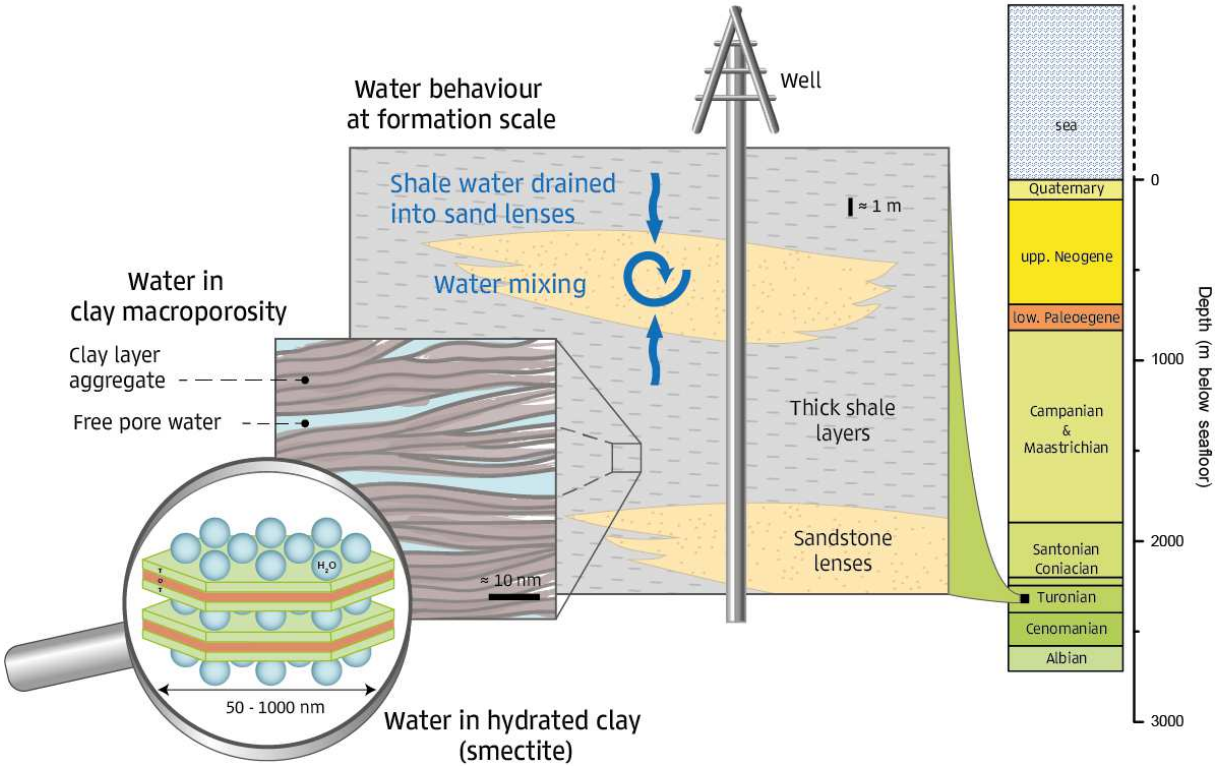

Figure 1: Schematic representation of the sediment geometry crossed by the well in the sediments of the Santonian, Coniacian and Turonian ages with sandstone lenses intercalated between thicker shale layers. Fluids expulsed from the shale are drained and mixed in the sandstone lenses. Water in the clayrock is distributed between the water in the macroporosity, expulsed by compaction, and the water in the interlayer space of smectite crystals, released during smectite dehydration.

Well data suggesting clay dehydration

Several chemical and isotopic parameters measured on the water sampled in different sandstone lenses after the borehole drilling suggest that clay dehydration occurred in the shale layers (Figure 2, Table 5). A salinity decrease is observed with increasing depth, where the total dissolved salt (TDS)

content decreases from 18 to 5 g/L between about 2000 m and 2600 m deep, below the seafloor. Concomitantly to this salinity decrease, an increase in the $\delta^{18}O$-H_2O isotopic signature is observed. The shallower water sample (sample 1 in Figure 2) has a $\delta^{18}O$-H_2O signature of +0.6 ‰ vs SMOW (Standard Mean Ocean Water), close to reference 0 ‰ $\delta^{18}O$-H_2O for seawater. The $\delta^{18}O$-H_2O signature increases up to +7.1 ‰ vs SMOW in the deeper water samples. This increase of the $\delta^{18}O$-H_2O signature can be explained by a release of positive $\delta^{18}O$ during clay dehydration or alteration ($\delta^{18}O$ of smectite ranges between +17 and +26 ‰ (Savin & Lee, 1988; Sheppard & Gilg, 1996)). Combined with the observed salinity decrease, the $\delta^{18}O$-H_2O signature evolution suggests a two-step evolution. First, the seawater trapped in the sediment is diluted without modifying its $\delta^{18}O$-H_2O isotopic signature. This dilution can be attributed to the water produced by the surrounding shale layers during compaction and possibly affected by ultrafiltration process (Kharaka & Berry, 1973). Secondly, the salinity of sandstone lenses continues to decrease together with an increase of the $\delta^{18}O$-H_2O. The smectite dehydration produces pure water with an elevated $\delta^{18}O$-H_2O signature causing the dilution and the rise of the $\delta^{18}O$-H_2O signature.

The δD-H_2O isotopic signature evolution (Figure 2) first shows a decrease from -9.5 ‰ to -19.1 ‰ between the two shallower samples 1 and 2 and then an increase to -13.4 ‰ for the deeper sample. The causes of δD-H_2O evolution are more complex to identify because δD varies over a large range of isotopic signatures in smectite (δD from -95 ‰ to +33 ‰ in smectite (Capuano, 1992; Savin & Epstein, 1970)) and the induced variation can be overprinted by other factors, such as the interaction with alkane gases or the degradation of organic matter.

Insights on the water-rock interactions are given by the water chemistry evolution. In Figure 3, the water composition is reported as ratio of reactive species content (Na, Ca, Mg and K) in relation to a conservative species content (Cl) to distinguish the reactive processes from transport and dilution processes. The increase with depth of the Na/Cl, Ca/Cl, Mg/Cl and K/Cl content ratio indicates the dissolution of primary mineral phases containing Na, Ca, Mg and K, such as feldspars, micas or clay minerals, not followed by large precipitations of aluminosilicate phases. This identified trend in the diagenesis in the sedimentary pile is confirmed by petrographic observations in samples that show only little precipitations of kaolinite as diagenetic formation of aluminosilicate phases. The main authigenic minerals being observed are quartz and calcite. The fluid chemistry evolution does not reflect smectite-to-illite transformation, with an observed increase with depth of the K content in relation to the Cl content, while a decrease is expected if K is used for illite formation. In addition, the only 3 mineralogical analyses performed on shale layers of the sedimentary pile do not show a decrease in smectite content and an increase in illite content in the interstratified illite/smectite. It

291 therefore appears that illitisation does not take place to a large extent and can be neglected in our
292 analysis.

293 No or little cross-formation flow in the sedimentary pile between the different sand lenses is
294 suggested by the $^{87}Sr/^{86}Sr$ isotopic ratio and the δ^7Li isotopic signature measured on the sampled
295 water (Figure 2). The $^{87}Sr/^{86}Sr$ isotopic ratio increases with depth, at values higher than the
296 theoretical $^{87}Sr/^{86}Sr$ ratio of Cenomanian seawater. This increase of the $^{87}Sr/^{86}Sr$ is likely to be due to
297 the alteration of feldspar and clay minerals that release strontium richer in ^{87}Sr, whose alteration
298 increases with depth. The δ^7Li isotopic signature in the water samples decreases with depth, from
299 +5.8 ‰ in the shallower water sample (sample 1) to +1.8 ‰ in the deepest sample. These δ^7Li
300 signatures are lower than the signature of modern seawater (+31 ‰ vs L-SVEC) and their range is
301 compatible with an interaction with minerals of sedimentary rocks, such as clays. The decrease of the
302 δ^7Li indicates the progress of the water/rock interaction with depth. The record of these progressive
303 increase of $^{87}Sr/^{86}Sr$ and decrease of δ^7Li indicate the absence of connexion or a restricted connexion
304 between the different sampled sand lenses. The hydrogeological media around each sand reservoir is
305 thus closed, with little water flow and transport between the sand lenses and the surrounding shale
306 layers (Figure 1).

307

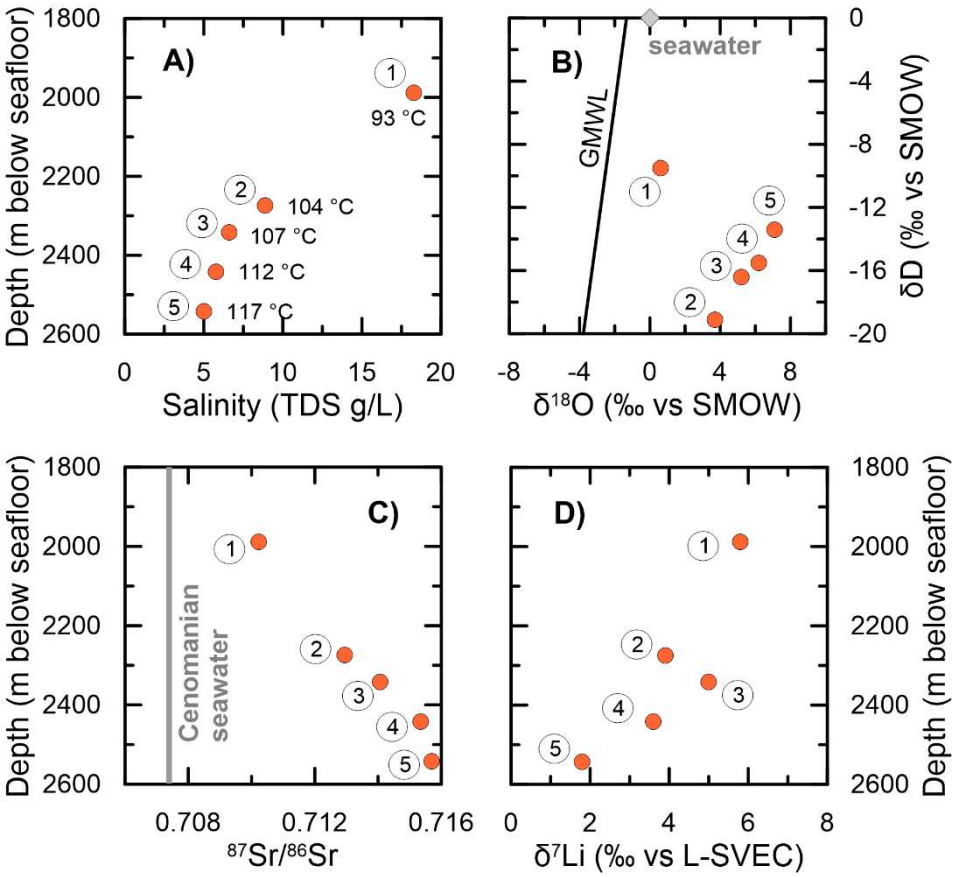

Figure 2: Data for water samples from the well showing: a) decreasing salinity with depth; b) δD as a function of the $\delta^{18}O$ water isotope signature at different depths. The reference seawater signature and the global meteoric water line (GMWL) are also shown; c) $^{87}Sr/^{86}Sr$ isotopic ratio increasing with depth and deviating from the ratio of the Cenomanian seawater; and d) $\delta^{7}Li$ isotopic signature decrease with depth. The circled numbers identify the five different water samples taken in the well.

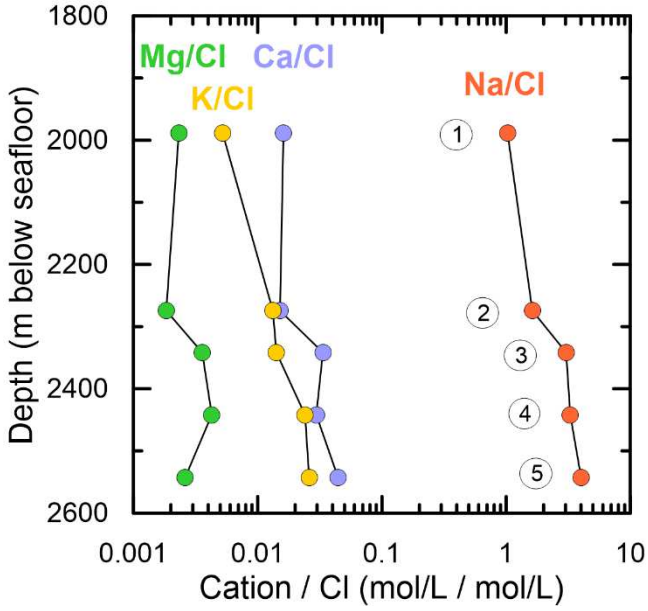

316 *Figure 3. Water chemistry data from the five water samples taken in the well in sand lenses (identified by circled numbers).*
317 *The evolution of the concentration ratios (Na/Cl, Ca/Cl, Mg/Cl and K/Cl) helps identified the water/rock interactions within*
318 *the sedimentary pile.*

319 *Table 5: Data from water samples taken at different depth in the well: temperature, chemical composition and isotopic*
320 *signatures.*

	Temperature (°C)	Salinity TDS (g/L)	$\delta^{18}O$-H_2O (‰ vs SMOW)	δD-H_2O (‰ vs SMOW)	$^{87}Sr/^{86}Sr$	δ^7Li (‰ vs LSVEC)	Na^+ (mg/L)	K^+ (mg/L)	Ca^{++} (mg/L)	Mg^{++} (mg/L)	Cl^- (mg/L)
Sample 1	93	18.27	+0.6	-9.5	0.7102	+5.8	5430	47	149	13	8177
Sample 2	104	8.89	+3.7	-19.1	0.7130	+3.9	2594	36	42	3.1	2461
Sample 3	107	6.61	+5.2	-16.4	0.7141	+5.0	1771	14	34	2.2	899
Sample 4	112	5.77	+6.2	-15.5	0.7153	+3.6	1522	19	24	2.1	717
Sample 5	117	5.02	+7.1	-13.4	0.7157	+1.8	1450	16	28	1.4	559

321

322

323 Model results – Reproducing the water isotope, salinity evolution and 324 overpressure considering smectite dehydration during sedimentary 325 pile burial

326 The water salinity and its isotopic composition in the sandstone lenses can be influenced by several
327 processes such as the expulsion of water during shale compaction, the release of water during
328 smectite dehydration and mixing of water from the sandstone and the shale. To individualise the
329 effect of smectite dehydration on the fluid evolution, it is necessary to consider these different
330 effects together and establish the water budget in the sedimentary pile. To this end, we calculated
331 the water production by smectite dehydration with a model reproducing the deposition of
332 sediments, the compaction of these sediments, the temperature increase with burial and the water
333 flow and pressure evolution in the sedimentary pile (Tremosa et al., 2020).

334 Burial and smectite dehydration

335 Our 1D forward modelling of sediment burial is performed based on the present-day lithological log
336 that identifies the thickness and lithology of the successive deposited lithological layers and on the
337 dating of stratigraphic surfaces that allows varying sedimentation rates to be calculated over time.
338 Sedimentation, compaction and pressure and temperature evolution in the sedimentary pile are then
339 reproduced since the Albian (Figure 5). Burial simulation coherence is assessed by comparison with
340 the present-day recorded thickness, porosity and temperatures profiles.

The calculated temperature and pressure evolutions over time allow the smectite dehydration model to be applied (Tremosa et al., 2020; Vidal & Dubacq, 2009). This model describes smectite dehydration as three possible binary solid solutions between hydrated and dehydrated smectite end-members. The hydrated smectite can have 1, 2 or 3 layers of water in the smectite interlayer space, depending on the calculated thermodynamic stability of each hydrated smectite for given temperature and pressure conditions. With increasing temperature, smectite dehydrates according to the most stable solid solution between hydrated and dehydrated smectite. However, at the temperature transition between two stability domains of solid solutions, a consequent release of water occurs because hydrated smectite loses one full layer of interlayer water. The thermodynamic model is based on the standard state properties of hydrated and dehydrated smectite end-members and integrates excess parameters for non-ideal solid solutions. Its results are in fair agreement with the smectite dehydration experiments (Vidal & Dubacq, 2009). The release of water by smectite dehydration is then simulated over the geological time across the investigated sedimentary pile (Figure 4).

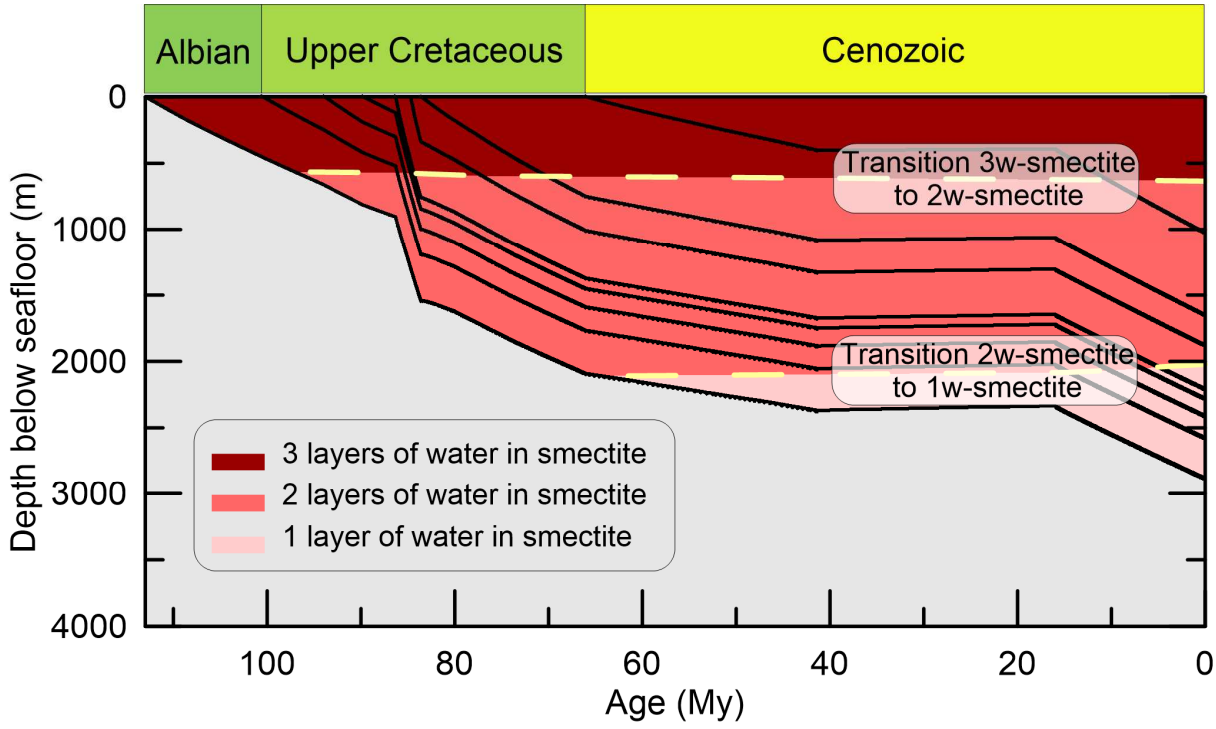

Figure 4: Evolution of the stable hydrated solid solution end-member in the smectite dehydration model as a function of sediment burial from the Albian to the present day. The black lines correspond to the depth evolution over time of the different stratigraphic surfaces and the grey area to the basement of the sedimentary pile, taken from the modelled domain.

Pressure profile

Pore pressure evolves in the sedimentary pile because of sediment compaction which induces a porosity reduction and a compression of the water filling the pores, water expansion during

temperature increase, water release by smectite dehydration and advective water flow. An overpressure of 150 to 170 bar is observed in the Turonian reservoirs at a depth of around 2500 m below the seafloor. The model that considers smectite dehydration in addition to compaction and temperature increase reproduces the present-day pressure profile (Figure 5). When smectite dehydration is omitted in the model, the pressure is about 40 bar lower, indicating that smectite dehydration contributes to about 25 % of the recorded overpressure. The model indicates that the overpressure is generated during the last burial episode that started 16 My ago. The transition of smectite hydrated with two layers of water to one layer of water is crossed in the Cenomanian to Santonian layers during this burial event (Figure 4), leading to a consequent release of water that contributes to the pore pressure.

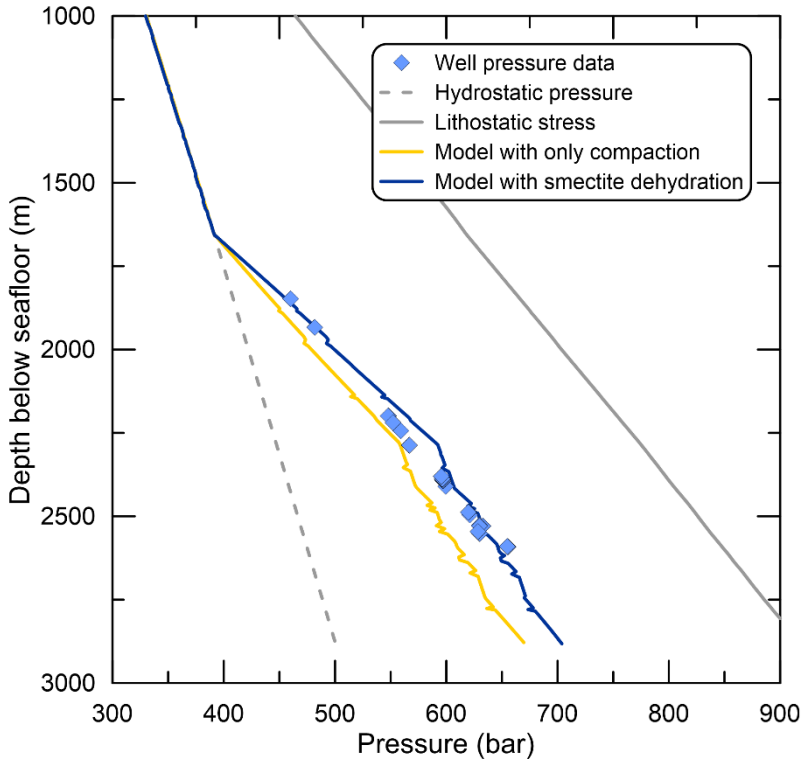

Figure 5: Measured and calculated pressure profiles at present day, with and without smectite dehydration in addition to compaction. Hydrostatic and overburden pressures are shown for comparison.

Chemical and isotopic evolution of fluids

The evolution of the chemical and isotopic composition of water in the sandstone lenses is calculated by mixing, in the sandstone levels, the water originated from the surrounding shale layers, in order to respect the water balance within the geometry and the evolution of the considered sedimentary pile. Dilution of the initial seawater in the sandstone lenses by compaction water flowing from the shale layers or produced by smectite dehydration is simulated when intrinsic permeability of overlying shale drops below 10^{-20} m², by effect of compaction. This criterion on the permeability of the shale

assumes that the hydrogeological media formed of a sandstone lens and its surrounding shale layers becomes closed to external flow below this permeability. It corresponds to a burial depth of about 1900 m and to the depth of the overpressure roof in the present-day pressure profile.

The water isotopic signature remains unchanged during the dilution by compaction water because the water trapped in the porosity of both shale and sandstone sediments was seawater with a $\delta^{18}O$-H_2O signature of 0 ‰. Besides, smectite dehydration releases water with a positive $\delta^{18}O$-H_2O signature of +20 ‰ SMOW, in agreement with the $\delta^{18}O$ signature of smectite referenced in the literature (Savin & Lee, 1988; Sheppard & Gilg, 1996).

The model considering smectite dehydration during basin burial reproduces, in good agreement, the related evolution with a depth of $\delta^{18}O$-H_2O signature and salinity of sampled water from sandstone levels in the well (Figure 6). During the modelling of the burial, the salinity in the sandstone layer corresponding to the deepest sampled sandstone lens first decreases due to seawater dilution without changing its isotopic signature and then decreases together with an increase in the $\delta^{18}O$ signature of water. The model captures the effect of releasing water with positive $\delta^{18}O$ during smectite dehydration. The mixing of this released water in the associated sandstone level follows the measured $\delta^{18}O$-H_2O signature to obtain a $\delta^{18}O$-H_2O of +6.8 ‰ for the deepest sampled sandstone lens. The transition of a hydrated smectite with 2 layers of water to 1 layer of water is modelled at a depth between the first and the second sampled sandstone lenses, with the associated freshening calculated. It is worth noting that the $\delta^{18}O$-H_2O signature and salinity evolution are obtained for the corresponding shale and sandstone thickness, smectite content in shale and timing of smectite dehydration.

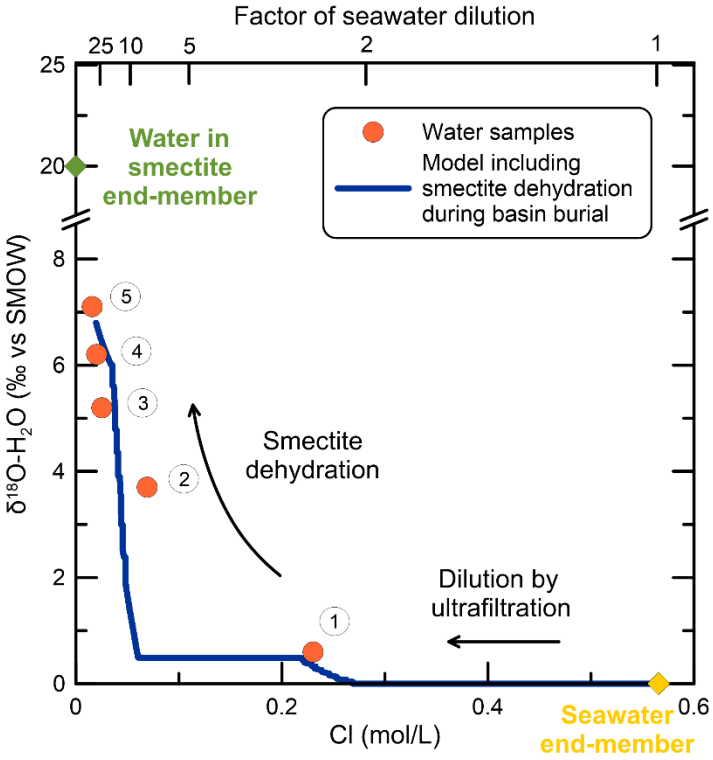

Figure 6: $\delta^{18}O$-H_2O isotopic signature compared to the salinity (concentration of chlorine) of the sampled water in sandstone lenses of the well. The model accounting for smectite dehydration during basin burial reproduces the evolution of water samples observed with depth. The salinity decrease is also shown as a factor of seawater dilution. Circled numbers correspond to the water samples, as in Figure 2.

Discussion

First evidence of smectite dehydration at the scale of the sedimentary pile

The present results constitute the first consistent evidence of the influence of smectite dehydration on the fluid salinity and pressure in a sedimentary basin. The model coherence in reproducing the $\delta^{18}O$-H_2O isotopic signature, the salinity and the pressure profile supports this influence of smectite dehydration. Up to now, the influence of smectite dehydration was advanced for the evolution of the chemical composition and isotopic signature of the sediments porewater (Hanor, 1994) or for its contribution to the fluid overpressure (Tremosa et al., 2020), but both effects were not simulated together. The burial of Cretaceous sediments was modelled in the Gulf of Guinea and the fluid pressure and smectite dehydration were simulated during this burial. Calculations showed that smectite dehydration explains about a quarter of the present-day recorded overpressure, in addition to disequilibrium compaction and temperature increase. Water freshening caused by ultrafiltration flow and by smectite dehydration can reproduce the salinity evolution with depth in sandstone lenses surrounded by thick shale layers. The salinity decrease is accompanied by an increase in the $\delta^{18}O$-H_2O signature that exactly matches the $\delta^{18}O$-H_2O signature evolution modelled by the release of

423 water by smectite dehydration during the burial of the sedimentary pile, where the water budget
424 during smectite dehydration and its timing are respected.

425 Uncertainties on the isotopic signature of smectite interlayer water

426 A calculation hypothesis was made on the $\delta^{18}O$ signature of the water released during smectite
427 dehydration. Relatively few data are available on the $\delta^{18}O$ signature of smectite and these signatures
428 can present some contamination because of the difficulties in purifying smectite and clay minerals
429 (Sheppard & Gilg, 1996). However, $\delta^{18}O$ signatures for smectite ranging between +17 and +26 ‰
430 (Savin & Lee, 1988) seem reasonable. It is more difficult to estimate the $\delta^{18}O$ signature of smectite
431 interlayer water because the interlayer water can be lost during sample preparation or interstitial
432 water can remain sorbed on the clay mineral (Sheppard & Gilg, 1996). In the literature, it has been
433 claimed that the exchange between porewater and interlayer water is fast and that the δD and $\delta^{18}O$
434 signatures of interlayer water do not provide geological information (Savin & Epstein, 1970).
435 However, this affirmation is in disagreement with studies on the interstitial water of mud volcanoes
436 that showed a clear influence of smectite dehydration on their water isotope signature (Dählmann &
437 Lange, 2003; Hensen et al., 2007) and rather suggest that the $\delta^{18}O$ signature of interlayer water is
438 close to the $\delta^{18}O$ signature of structural smectite. The distinction between structural and interlayer
439 $\delta^{18}O$ isotopic signatures hence remains to be investigated, by dedicated experiments in order to
440 distinguish between the production of pore and interlayer water in a smectite (Fernández et al.,
441 2014) or from insights given by molecular dynamics simulations.

442 Discarding other sources of water isotopic signature variations

443 The influence on the $\delta^{18}O$-H_2O isotopic signature evolution of other water-rock interaction
444 (carbonate precipitation and smectite illitisation) or transport (ultrafiltration) processes can be
445 discarded in the sedimentary system under consideration. The isotopic fractionation during the
446 precipitation of carbonate minerals is known to modify the $\delta^{18}O$-H_2O isotopic signature. In the
447 studied lithological column, petrographic observations indicate an early cementation of calcite,
448 during the early stage of burial and compaction, at temperature estimated at about 30°C. If the $\delta^{18}O$-
449 H_2O isotopic signature has been modified at that time because of calcite precipitation, it occurred in
450 a hydraulic open system, where water can be flushed. The simulation scenario considers the dilution
451 and isotopic shift when the system becomes closed on a hydraulic point of view, namely, when the
452 intrinsic permeability of the overlying shale layer becomes lower than 10^{-20} m^2, corresponding to a
453 burial depth of about 1900 m. Hence, the precipitation of early carbonates is not expected to change
454 the calculated $\delta^{18}O$-H_2O evolution since this precipitation occurred before. The isotopic fractionation
455 during the smectite-to-illite transformation can also lead to an increase of the $\delta^{18}O$-H_2O isotopic

signature at increasing temperature (Suchecki & Land, 1983). The data on mineralogy and water chemistry available from the well indicate an absence of noticeable illitisation. Consequently, the recorded $\delta^{18}O$-H_2O isotopic signature in the sand lenses is certainly not impacted by smectite illitisation process. During ultrafiltration flow, a flow of water with solute transport partially impeded because of the membrane behaviour of the shale, a moderate isotopic fractionation can occur (Agrinier et al., 2021; Coplen & Hanshaw, 1973). However, the effect of this isotopic fractionation during ultrafiltration is not clearly established, with contradictory studies reporting a depletion or an enrichment of the $\delta^{18}O$-H_2O signature of the water flowing out of the shale (Agrinier et al., 2021). The effect of ultrafiltration on $\delta^{18}O$-H_2O isotopic signature is difficulty distinguished from the effect of water-rock interactions. In the simulations executed in the present study, a flow of fresh water expulsed from the shale layers that can correspond to ultrafiltration is mimicked by considering a progressive dilution of the water in the sand lenses. Since the effect of ultrafiltration on the $\delta^{18}O$-H_2O isotopic signature remains unclear and probably weak and because the simulation of ultrafiltration process is complex, this possible effect has not been considered in this analysis.

Likely occurrence of smectite dehydration compared to illitisation

In studies on fluid evolution or overpressure generation by the water released by smectite, the analysis is often restricted to smectite-to-illite transformation, but more rarely consider the dehydration of interlayer smectite, notwithstanding that interlayer dehydration is thermodynamically and kinetically easier than illitisation. However, even in high pressure environments in which the total dehydration is predicted at a temperature of 300°C or higher, the main dehydration steps (3 layers of water to 2 and 2 layers of water to 1) take place at temperatures lower than 150°C (Vidal & Dubacq, 2009), concomitantly to smectite illitisation. The formation of illite consumes potassium and, then, a depletion of potassium in the porewater indicates the occurrence of a significant illitisation. In the present study, such a marker of illitisation was not observed from the K/Na ratio and smectite-to-illite transformation was ruled out. At the contrary, when the porewater composition shows a consumption of potassium (Vanneste et al., 2011), smectite illitisation is rationally to consider in the fluid budget analysis.

Implications on fluid budget in sedimentary basins

Our demonstration of the identification of smectite dehydration as the source of fluid modification in the studied sedimentary pile in the Gulf of Guinea highlights the importance of considering coupled approaches to understand the origin of fluids in sedimentary basins. Assessing the fluid budget in a sedimentary basin requires dedicated and integrated studies accounting for the temporal and spatial production of fluid and using a sound and calibrated model of fluid production. Notably, the water

release during smectite dehydration was calculated using a predictive thermodynamic model calibrated on experimental data. Thanks to this approach, it is possible to use the water's isotopic evolution as a hydrogeological constraint in regional studies of fluid migration.

Conclusions

Smectite dehydration was advanced as a process that can influence the fluid pressure and the water composition and isotopic signature in sedimentary basins, but a direct evidence has been lacking up to now. In the sedimentary pile studied in the Gulf of Guinea, the dehydration of smectite interlayer water influences the overpressure and the porewater composition and isotopic signature. This influence was evidenced thanks to the simulation of the water production during the burial using a modelling approach that couples hydraulic, mechanical, thermal, thermodynamic and isotopic processes. In the model, smectite dehydration is described using a thermodynamic model and driven by the temperature and pressure changes during the burial where the volume of water released depends on the geometry of the sedimentary pile. This spatial and temporal fluid budget shows that smectite dehydration contributes to about 25 % of the present-day overpressure of 150 to 170 bar, together with classical purely hydro-mechanical processes. In addition to influence the overpressure, smectite dehydration induces a dilution of porewater salinity and an increase of the $\delta^{18}O$-H_2O isotopic signature with increasing depth. Unique data from a deep well of more than 5000 m of total depth, including 2000 m of water, were used in our analysis. The simulation of these hydraulic, chemical and isotopic markers are goods clues of the on-going geological process in the sedimentary basin.

The influence of smectite dehydration is specific to each sedimentary system and evaluating the contribution of smectite dehydration requires performing a water budget involving smectite dehydration during the burial of the studied sedimentary pile. Our study is focused on the evaluation of fluid migration in sedimentary basins for the potential exploitation of energy fluids but it is also of interest to have a better understanding of the effect of smectite dehydration in other contexts. For example, our findings and the methodology undertaken here can be directly be applied in studies on the behaviour of fluids in subduction zones or in mud volcanoes.

Acknowledgments

This work was funded by TOTAL S.A. and BRGM. Céline Roux is thanked for the figure artwork and Sally Ferguson for the English language editing. Editor M. Kersten and one anonymous reviewer are acknowledged for their constructive comments on the manuscript.

Author contributions

J.T. adapted a previous version of the SURP code, made the coupled modelling and interpreted the results. H.G. calculated the thermodynamic parameters describing smectite dehydration. E.C.G. took the water samples, ordered the isotopic and chemical analysis and emitted the hypothesis that the isotopic and salinity data reflected smectite dehydration. J.T. wrote the early version of the manuscript. E.C.G. and H.G. contributed to the writing of the manuscript. All authors participated to conceptualize this study and commented on the final version of the manuscript

References

Agrinier, P., Bonifacie, M., Bardoux, G., Lucazeau, F., Giunta, T., & Ader, M. (2021). Chlorine isotope data of chlorides challenge the pore fluid paradigm. *Geochimica Cosmochimica Acta*, *300*, 258–278. https://doi.org/10.1016/j.gca.2021.02.034

Antobreh, A. A., Faleide, J. I., Tsikalas, F., & Planke, S. (2009). Rift–shear architecture and tectonic development of the Ghana margin deduced from multichannel seismic reflection and potential field data. *Marine and Petroleum Geology*, *26*(3), 345–368. https://doi.org/10.1016/j.marpetgeo.2008.04.005

Audet, D. M. (1995). Mathematical modelling of gravitational compaction and clay dehydration in thick sediment layers. *Geophysical Journal International*, *122*(1), 283–298. https://doi.org/10.1111/j.1365-246X.1995.tb03554.x

Bekins, B. A., McCaffrey, A. M., & Dreiss, S. J. (1995). Episodic and constant flow models for the origin of low-chloride waters in a modern accretionary complex. *Water Resources Research*, *31*(12), 3205–3215. https://doi.org/10.1029/95WR02569

543 Bjørlykke, K., Jahren, J., Aagaard, P., & Fisher, Q. (2010). Role of effective permeability distribution in
544 estimating overpressure using basin modelling. *Marine and Petroleum Geology*, *27*(8), 1684–
545 1691. https://doi.org/10.1016/j.marpetgeo.2010.05.003
546 Blanc, P., Vieillard, P., Gailhanou, H., Gaboreau, S., Gaucher, E., Fialips, & Giffaut, E. (2015). A
547 generalized model for predicting the thermodynamic properties of clay minerals. *American*
548 *Journal of Science*, *315*, 734–780.
549 Boschetti, T., Angulo, B., Cabrera, F., Vásquez, J., & Montero, R. L. (2016). Hydrogeochemical
550 characterization of oilfield waters from southeast Maracaibo Basin (Venezuela): Diagenetic
551 effects on chemical and isotopic composition. *Marine and Petroleum Geology*, *73*, 228–248.
552 https://doi.org/10.1016/j.marpetgeo.2016.02.020
553 Brown, K. M., Saffer, D. M., & Bekins, B. A. (2001). Smectite diagenesis, pore-water freshening, and
554 fluid flow at the toe of the Nankai wedge. *Earth and Planetary Science Letters*, *194*(1), 97–
555 109. https://doi.org/10.1016/S0012-821X(01)00546-5
556 Bruce, C. H. (1984). Smectite dehydration; its relation to structural development and hydrocarbon
557 accumulation in northern Gulf of Mexico basin. *AAPG Bulletin*, *68*, 673–683.
558 Capuano, R. . (1992). The temperature dependence of hydrogen isotope fractionation between clay
559 minerals and water: Evidence from a geopressured system. *Geochimica et Cosmochimica*
560 *Acta*, *56*(6), 2547–2554. https://doi.org/10.1016/0016-7037(92)90208-Z
561 Clayton, R. N., Friedman, I., Graf, D. L., Mayeda, T. K., Meents, W. F., & Shimp, N. F. (1966). The origin
562 of saline formation waters: 1. Isotopic composition. *Journal of Geophysical Research*, *71*(16),
563 3869–3882. https://doi.org/10.1029/JZ071i016p03869
564 Colten-Bradley, V. A. (1987). Role of pressure in smectite dehydration; effects on geopressure and
565 smectite-to-illite transformation. *AAPG Bulletin*, *71*, 1414–1427.
566 Coplen, T. B., & Hanshaw, B. B. (1973). Ultrafiltration by a compacted clay membrane—I. Oxygen and
567 hydrogen isotopic fractionation. *Geochimica Cosmochimica Acta*, *37*(10), 2295–2310.
568 https://doi.org/10.1016/0016-7037(73)90105-1

569 Dählmann, A., & Lange, G. . de. (2003). Fluid–sediment interactions at Eastern Mediterranean mud
570 volcanoes: a stable isotope study from ODP Leg 160. *Earth and Planetary Science Letters*,
571 *212*(3), 377–391. https://doi.org/10.1016/S0012-821X(03)00227-9
572 Fernández, A. M., Sánchez-Ledesma, D. M., Tournassat, C., Melón, A., Gaucher, E. C., Astudillo, J., &
573 Vinsot, A. (2014). Applying the squeezing technique to highly consolidated clayrocks for pore
574 water characterisation: Lessons learned from experiments at the Mont Terri Rock Laboratory.
575 *Applied Geochemistry*, *49*, 2–21. https://doi.org/10.1016/j.apgeochem.2014.07.003
576 Fitts, T. G., & Brown, K. M. (1999). Stress-induced smectite dehydration: ramifications for patterns of
577 freshening and fluid expulsion in the N. Barbados accretionary wedge. *Earth and Planetary*
578 *Science Letters*, *172*(1), 179–197. https://doi.org/10.1016/S0012-821X(99)00168-5
579 Franks, S. G., & Uchytil, S. J. (2016). Geochemistry of formation waters from the subsalt Tubular Bells
580 Field, offshore Gulf of Mexico: Implications for fluid movement and reservoir continuity.
581 *AAPG Bulletin*, *100*(6), 943–967. https://doi.org/10.1306/02101615027
582 Hanor, J. S. (1994). Physical and chemical controls on the composition of waters in sedimentary
583 basins. *Marine and Petroleum Geology*, *11*(1), 31–45. https://doi.org/10.1016/0264-
584 8172(94)90007-8
585 Henry, P., & Bourlange, S. (2004). Smectite and fluid budget at Nankai ODP sites derived from cation
586 exchange capacity. *Earth and Planetary Science Letters*, *219*(1), 129–145.
587 https://doi.org/10.1016/S0012-821X(03)00694-0
588 Hensen, C., Nuzzo, M., Hornibrook, E., Pinheiro, L. M., Bock, B., Magalhães, V. H., & Brückmann, W.
589 (2007). Sources of mud volcano fluids in the Gulf of Cadiz—indications for hydrothermal
590 imprint. *Geochimica et Cosmochimica Acta*, *71*(5), 1232–1248.
591 https://doi.org/10.1016/j.gca.2006.11.022
592 Hüpers, A., & Kopf, A. J. (2012). Effect of smectite dehydration on pore water geochemistry in the
593 shallow subduction zone: An experimental approach. *Geochemistry, Geophysics, Geosystems*,
594 *13*(10). https://doi.org/10.1029/2012GC004212

595 Hüpers, A., Grathoff, G., Warr, L. N., Wemmer, K., Spinelli, G., & Underwood, M. B. (2019).
596 Spatiotemporal Characterization of Smectite-to-Illite Diagenesis in the Nankai Trough
597 Accretionary Prism Revealed by Samples From 3 km Below Seafloor. *Geochemistry,*
598 *Geophysics, Geosystems*, *20*(2), 933–951. https://doi.org/10.1029/2018GC008015
599 Kastner, M. J., Elderfield, H., Jenkins, W. J., Gieskes, J. M., & Gamo, T. (1993). Geochemical and
600 isotopic evidence for fluid flow in the western Nankai subduction zone, Japan. In *Proceedings*
601 *of the Ocean Drilling Program, Scientific Results, Vol. 131*.
602 Kharaka, Y. K., & Berry, F. A. P. (1973). Simultaneous flow of water and solutes through geological
603 membranes—I. Experimental investigation. *Geochimica et Cosmochimica Acta*, *37*(12), 2577–
604 2603. https://doi.org/10.1016/0016-7037(73)90267-6
605 Macpherson, G. L. (1992). Regional Variations in Formation Water Chemistry: Major and Minor
606 Elements, Frio Formation Fluids, Texas. *AAPG Bulletin*, *76*(5), 740–757.
607 https://doi.org/10.1306/BDFF88C6-1718-11D7-8645000102C1865D
608 Mascle, J., & Blarez, E. (1987). Evidence for transform margin evolution from the Ivory Coast-Ghana
609 continental margin. *Nature*, *326*(6111), 378–381. Retrieved from
610 https://doi.org/10.1038/326378a0
611 Meunier, A., & Velde, B. (1989). Solid solution in I/S mixed-layer minerals and illite. *American*
612 *Mineralogist*, *74*, 1106–1112.
613 Morton, R. A., & Land, L. S. (1987). Regional Variations in Formation Water Chemistry, Frio Formation
614 (Oligocene), Texas Gulf Coast1. *AAPG Bulletin*, *71*(2), 191–206.
615 https://doi.org/10.1306/94886D6C-1704-11D7-8645000102C1865D
616 Neuzil, C. E. (1995). Abnormal pressures as hydrodynamic phenomena. *American Journal of Science*,
617 *295*, 742–786.
618 Nicot, J.-P., Gherabati, A., Darvari, R., & Mickler, P. (2018). Salinity Reversal and Water Freshening in
619 the Eagle Ford Shale, Texas, USA. *ACS Earth and Space Chemistry*, *2*(11), 1087–1094.
620 https://doi.org/10.1021/acsearthspacechem.8b00095

621 Saffer, D. M., & McKiernan, A. W. (2009). Evaluation of in situ smectite dehydration as a pore water
622 freshening mechanism in the Nankai Trough, offshore southwest Japan. *Geochemistry,*
623 *Geophysics, Geosystems*, *10*(2). https://doi.org/10.1029/2008GC002226
624 Savin, S. M., & Epstein, S. (1970). The oxygen and hydrogen isotope geochemistry of clay minerals.
625 *Geochimica et Cosmochimica Acta*, *34*(1), 25–42. https://doi.org/10.1016/0016-
626 7037(70)90149-3
627 Savin, S. M., & Lee, M. (1988). Hydrous phyllosilicates. In S. W. Bailey (Ed.) (Vol. 19, pp. 189–223).
628 Mineralogical Society of America.
629 Sclater, J. G., & Christie, P. A. F. (1980). Continental stretching: An explanation of the Post-Mid-
630 Cretaceous subsidence of the central North Sea Basin. *Journal of Geophysical Research: Solid*
631 *Earth*, *85*(B7), 3711–3739. https://doi.org/10.1029/JB085iB07p03711
632 Sheppard, S. M. F., & Gilg, H. A. (1996). Stable isotope geochemistry of clay minerals: "The story of
633 sloppy, sticky, lumpy and tough" Cairns-Smith (1971). *Clay Minerals*, *31*(1), 1–24.
634 https://doi.org/10.1180/claymin.1996.031.1.01
635 Suchecki, R. K., & Land, L. S. (1983). Isotopic geochemistry of burial-metamorphosed volcanogenic
636 sediments, Great Valley sequence, northern California. *Geochimica Cosmochimica Acta*,
637 *47*(8), 1487–1499. https://doi.org/10.1016/0016-7037(83)90308-3
638 Tanikawa, W., Shimamoto, T., Wey, S., Lin, C., & Lai, W. (2008). Stratigraphic variation of transport
639 properties and overpressure development in the Western Foothills, Taiwan. *Journal of*
640 *Geophysical Research: Solid Earth*, *113*(B12). https://doi.org/10.1029/2008JB005647
641 Tremosa, J., Gailhanou, H., Chiaberge, C., Castilla, R., Gaucher, E. C., Lassin, A., … Claret, F. (2020).
642 Effects of smectite dehydration and illitisation on overpressures in sedimentary basins: A
643 coupled chemical and thermo-hydro-mechanical modelling approach. *Marine and Petroleum*
644 *Geology*, *111*, 166–178. https://doi.org/10.1016/j.marpetgeo.2019.08.021
645 Vanneste, H., Kelly-Gerreyn, B. A., Connelly, D. P., James, R. H., Haeckel, M., Fisher, R. E., … Mills, R.
646 A. (2011). Spatial variation in fluid flow and geochemical fluxes across the sediment–

seawater interface at the Carlos Ribeiro mud volcano (Gulf of Cadiz). *Geochimica et Cosmochimica Acta*, *75*(4), 1124–1144. https://doi.org/10.1016/j.gca.2010.11.017

Vidal, O., & Dubacq, B. (2009). Thermodynamic modelling of clay dehydration, stability and compositional evolution with temperature, pressure and H2O activity. *Geochimica et Cosmochimica Acta*, *73*(21), 6544–6564. https://doi.org/10.1016/j.gca.2009.07.035

Wilkinson, M., Crowley, S. F., & Marshall, J. D. (1992). Model for the evolution of oxygen isotope ratios in the pore fluids of mudrocks during burial. *Marine and Petroleum Geology*, *9*(1), 98–105. https://doi.org/10.1016/0264-8172(92)90007-2